Exciton-phonon scattering and nonradiative relaxation of excited carriers in hydrothermally synthesized CdTe quantum dots

Amardeep M Jagtap[1], Jayakrishna Khatei[1,2], K S R Koteswara Rao[1*]

1. Department of Physics, Indian Institute of Science, Bnagalore – 560012, India

2. State Institute and Schulich Faculty of Chemistry, Technion-Israel Institute of Technology, Haifa, Israel

*Email: ksrkrao@physics.iisc.ernet.in

Abstract

Naturally formed CdTe/CdS core/shell quantum dot (QDs) structures in the presence of surface stabilizing agent have seen synthesized by hydrothermal method. Size and temperature dependent photoluminescence (PL) spectra have been investigated to understand the exciton-phonon interaction, radiative and nonradiative relaxation of carriers in these QDs. PL of these aqueous CdTe QDs (3.0 − 4.8 nm) have been studied in the temperature range 15 − 300 K. The strength of the exciton-LO-phonon coupling, as reflected in the Huang−Rhys parameter 'S' is found to increase from 1.13 to 1.51 with QDs size varying from 4.8 to 3.0 nm. The PL linewidth (FWHM) increases with increase in temperature and found to have maximum in the case of QDs with 3.0 nm in size, where exciton-acoustic phonon coupling coefficient enhanced, 51 μeV/K compared to the bulk value of 0.72 μeV/K. To understand the nonradiative processes, which affect the relaxation of carriers, the integrated PL intensity is observed as a function of temperature. The integrated PL intensity remains constant till 50 K for relatively large QDs (3.9 − 4.8 nm) beyond which thermally activated process takes over. Below 150 K, a small activation

energy, $15 - 20$ meV is found to be responsible for the quenching of PL. Above 150 K, the thermal escape from the dot assisted by scattering with multiple longitudinal optical (LO) phonons is the main mechanism for the fast quenching of PL. Besides this high temperature quenching, interestingly for relatively smaller size QDs (3.4 – 3.0 nm), the PL intensity enhances as the temperature increases up to $90 - 130$ K, which is attributed to the emission of carriers from interface/trap states having activation energy in the range of $6 - 13$ meV.

1. Introduction

Semiconductor nanocrystals (SNCs) or quantum dots (QDs) demonstrate a wide range of novel physical phenomena because of discretization of electronic density of states as a result of strong spatial confinement of carriers in these quasi-0D systems.[1-3] These SCNs have attracted significant scientific interests both fundamental and in technological applications such as in the field of optoelectronic systems including photovoltaic devices, light emitting diodes (LEDs), biomedical fluorescent labeling and lasing action.[4-8] The temperature dependence of the photoluminescence (PL) and its insensitivity in the oxygen ambience has been studied in CdSe QDs with ZnS overlayer, which shows an attractive class of optical indicators in the luminescence thermometry applications.[9] A model considering three-level energy system has been used to understand the thermal equilibrium between dark and bright exciton states and nonradiative relaxation processes, which affects the PL intensity has been studied in CdSe QDs.[10] Meijerink and co-workers have reported the high temperature $(300 - 477$ K) luminescence quenching of colloidal QDs, where the intrinsic quenching of luminescence is discussed based on mechanism of thermally activated crossover and multiphonon relaxation.[11]

The effect of defects has been studied on carrier relaxation pathways and exciton dynamics on CdS nanobelts through temperature dependent and time resolved PL spectroscopy.[12] Temperature dependent PL has been thoroughly studied in near infrared emitting PbS and PbS/CdS core shell QDs and found to have different distribution of defects/traps affecting the carrier relaxation.[13] Temperature dependent emission properties of midinfrared emitting epitaxially grown PbTe/CdTe QDs have also been investigated and the effect of strain is considered in the PL emission peak.[14] Ghosh and co-workers have reported the room temperature ultrafast charge carrier relaxation and charge transfer dynamics of CdTe/CdS core shell structures studied by femtosecond transient absorption spectroscopy, where the carrier relaxation was found to be slower and the carrier lifetime was longer in the core-shell structures compared to the nascent QDs.[15] Nonradiative relaxation of carriers has been studied in organically capped pure CdTe SCNs grown by non-organometallic procedure.[16]

Recently, aqueous grown colloidal QDs and core shell structures have attracted a lot of interest because of their biological compatibility and technological applications.[17] Considering the improvement in the crystallinity, size distribution, which enhances the optical properties of these QDs, microwave irradiation or hydrothermal technique (autoclave) has been utilized extensively in the growth.[18] Such aqueous grown thiol capped CdTe QDs have shown excellent quantum yield (QY) up to 40 – 80 %.[18,19] One of the reason for such improvement in the QY is considered to be the formation of CdS epitaxial layer that acts as shell on CdTe because of the presence of surface stabilizing agent (thiol group) during the growth process.[19] In principle, lower lattice mismatch will help to reduce interface states and obtaining better optical properties.[20,21] Recently, Anirban Samanta et al. have reported enhanced PL efficiency by introducing CdS shell between CdTe QDs and ZnS shell for avoiding sharp lattice mismatch

which facilitated the crystal growth of core/shell/shell of CdTe/CdS/ZnS QDs.[22] In another

report, the shell of CdS has been sandwiched between CdSe QDs and ZnS outer shell allowing

the reduction of strain inside the nanocrystals as CdS has lattice parameter intermediate to those

of CdSe and ZnS.[23] Not only CdS has wider band gap (2.5 eV) compared to CdTe (1.5 eV) but

also the lattice parameter mismatch (3.6 %) to CdTe which is relatively small compared to ZnSe

(12.5 %) and ZnS (16.5 %).[19] Therefore the detailed knowledge of temperature on radiative and

nonradiative relaxation process occurring in these aqueous grown inorganic SNCs is needed for

achieving optimal performance in the fields of biological and optoelectronics. These carrier

relaxation processes limits the quantum efficiencies of these QDs which are particularly operated

at room temperature.

In this report we present our investigations on temperature dependent PL of CdTe

QDs capped naturally with CdS shell in the presence of surface stabilizing agent (thiol group)

grown under hydrothermal conditions. QDs of sizes 3.0 – 4.8 nm have been synthesized and

structurally studied by TEM and XRD, where formation of CdS shell on CdTe has been

confirmed by XRD and EDX. Huang-Rhys parameter 'S', which gives the strength of the

electron-phonon coupling is found to be increasing with decrease in the QDs size. Effect of

confinement is seen through increase in exciton-acoustic phonon coupling coefficient with

decrease in QDs size, which causes increase in homogeneous broadening of emission spectra as

a function of temperature 15 – 300 K. In the case of QDs of large size 3.9 – 4.8 nm, PL intensity

decreases with increase in temperature from 50 – 150 K. In the temperature region above 150 K

PL quenching is relatively fast (4.8 – 3.0 nm size QDs) due to thermal escape of carrier from the

dot assisted by scattering with multiple longitudinal optical (LO) phonons. Interestingly, for

small size QDs (3.0 – 3.4 nm), the PL intensity enhances as the temperature increases up to 90 –

130 K, which is attributed to emission of carriers from surface/interface states to core emitting states of CdTe QDs with 6 – 13 meV energy barrier.

2. Experimental section

2.1 Chemicals and synthesis of CdTe QDs

Cadmium chloride dried ($CdCl_2$, 95%) was purchased from Fisher scientific. Sodium tellurite (Na_2TeO_3 -100 mesh, 99%) was purchased from Sigma Aldrich. Sodium borohydride ($NaBH_4$, 98%) and trisodium citrate dihydrate ($C_6H_5O_7Na_3 \cdot 2H_2O$, 99%) were obtained from s d fine-Chem Ltd. 3-Mercaptopropionic acid (MPA, 99%) was purchased from Spectrochem Pvt. Ltd. CdTe quantum dots were synthesized by hydrothermal method as described elsewhere.[24] Briefly, 0.16 mmol of $CdCl_2$ was taken in 40 mL of deionized water, which was followed by 100 mg of $C_6H_5O_7Na_3 \cdot 2H_2O$, 0.04 mmol of Na_2TeO_3 and 0.38 mmol of 3-mercaptopropionic acid (MPA) keeping the mixture under constant magnetic stirring. Further, 50 mg of $NaBH_4$ was added for reducing Te^{4-} to Te^{2-}, and the pH was adjusted to 8 – 8.5. The molar ratio of Cd^{2+}, Te^{2-} and MPA was 1:0.25:2.4. After 15 minutes, the above precursor solution was transferred to 50mL teflon lined stainless still autoclave and transferred to oven maintained at 180 $^\circ$C. The time of synthesis varied in steps of 20, 25, 35, 40 and 43minutes to obtain different size QDs. These aqueous grown QDs were precipitated and washed with isopropyl alcohol and deionized water, removing all unreacted chemicals and free MPA from these samples. Thus obtained aqueous grown CdTe QDs were dispersed in water soluble polyvinyl alcohol (PVA) to obtain the films for further PL measurements.

2.2 Characterization

UV-VIS-NIR absorption spectra on these colloidal QDs were recorded on Perkin Elmer Lambda unit. X-ray diffraction pattern were recorded on QDs powder with the help of RIGAKU SMARTLAB using Cu Kα radiation of 1.54 Aº. TEM and high resolution TEM (HRTEM) imaging were carried out on samples made by drop casting 3 μL QDs on holey carbon coated copper grid with Tecnai TM G2 F30 and FEI Tecnai T20 U-TWIN. Elemental composition was determined by performing EDX with the help of FEI Tecnai T20 U-TWIN. Room temperature time resolved PL studies were carried out on time correlated single photon counting (TCSPC) mode of Horiba scientific (FluroHub) using 469 nm emission line, LED (picoseconds) as excitation source. Low temperature PL measurements were carried out by Triax 550 monochromator assisted by photomultiplier tube as detector. Ar^+ laser tuned to 514.5 nm with power <1 mW was used for exciting the samples. Continuous liquid helium flow technique assisted by Janis cryostat and Lakeshore temperature controller-332 were used for tuning the sample temperature in the range of 15 – 300 K.

3. Results and discussion

3.1 Optical and structural properties

Fig. 1 shows UV-VIS absorption spectra of CdTe QDs synthesized under different lengths of time. The observed first excitonic absorption peak is at 546, 571, 610, 640 and 655 nm for 20, 25, 35, 40 and 43 minutes of synthesis, respectively. Structural characterization of the QDs carried out by TEM and HRTEM is shown in Fig. 2 for QDs synthesized 25 and 40 minutes (Other size QDs, Fig. S1)). The average sizes determined from TEM are 3.0, 3.4, 3.9, 4.3 and 4.8 nm for QDs synthesized for 20, 25, 35, 40 and 43 minutes, respectively. The size determined

from TEM and the energy gap considering the spectral position of first excitonic absorption peak

of these QDs are in good agreement with the earlier reports on CdTe QDs (Fig. S2). HRTEM

images (Fig. 2(C) and (D)) clearly show the interplanar spacing of 0.37 nm, which corresponds

to (111) plane of cubic zinc blende structure of CdTe.[25] XRD pattern in Fig. 3 clearly shows the

reflection peaks, which corresponds to (111), (220) and (311) planes of CdTe.[26] Interestingly,

these reflection peaks red shifts as the size of QDs increases from 3.0 to 4.8 nm. The shift is

attributed to the formation of naturally sulphur capped surface (CdS shell), which forms because

of mercapto-group (thiol) of surface stabilizing ligand MPA covalently attaching to the surface

cadmium atoms of CdTe QDs during hydrothermal growth process.[27] Thus such aqueous grown

MPA capped CdTe QDs represent a natural core-shell system. Further to confirm the sulphur

enriched shell of QDs, the elemental analysis carried out using EDX (Table S1†). The observed

content of sulphur is found to be between 22 − 42 % for the QDs (3.0 − 4.8 nm), which is

consistent with our XRD results. Thus the covalent binding of thiol groups to Cd atoms on QDs

surface can help to remove the dangling bonds and passivate the surface states.[27]

3.2 Temperature dependent photoluminescence studies

Temperature dependent PL of QDs is taken at intervals of 5 K up to 70 K beyond which10 K

step is used. Fig. 4 shows a typical PL spectra and their evolution as a function of temperature 15

− 300 K for 3.9 nm QDs (Other size QDs PL, Fig. S3). As the temperature increases, there is red

shift in the emission peak. In general, the line-width (FWHM) of the spectra increases while the

integrated PL intensity decreases with increase in the temperature (Fig. 4(B)). Fig. 5 shows the

change in the position of emission peak, which represents the energy gap as a function of

temperature for QDs of different sizes. It can be seen that the energy gap of QDs decreases (65 – 80 meV) with increase in temperature from 15 – 300 K. This temperature dependent behavior of energy gap for bulk semiconductors and their nanostructures is usually described by the semiempirical formula, known as Varshini relation.[28,29] Fig. 5(A) shows the data fitted with Varshini relation for all sizes of QDs (eqn (1)).

$$E_g(T) = E_{g0} - \alpha \frac{T^2}{(T + \beta)}. \qquad (1)$$

Where E_{g0} is the energy at 0 K, α is the temperature coefficient and β is close to Debye temperature θ_D of a given material. The best fit parameters obtained for α by keeping β fixed from bulk (158 K) are $(3.2 - 4.5) \times 10^{-4}$ eV/K. These values are in close agreement with the reported value of bulk CdTe ($\alpha \sim (3.0 - 4.1) \times 10^{-4}$ eV/K)[30] and organically capped CdTe nanocrystals ($\alpha \sim 3.2 \times 10^{-4}$ eV/K).[16] Thus, this result infers the reduction of QDs bandgap is similar to the bulk one, whereas the quantum confinement energies of carriers are not affected by the temperature.[31] The following equation [O'Donnell and Chen][32] determines the electron-phonon coupling in QDs, which involves the parameters that are related to the intrinsic interaction within the semiconductors.

$$E_g(T) = E_{g0} - \frac{2S\langle\hbar\omega\rangle}{e^{\frac{\langle\hbar\omega\rangle}{k_BT}} - 1}. \qquad (2)$$

Where S is the Huang-Rhys factor, $\langle\hbar\omega\rangle$ is the average phonon energy and k_B is the Boltzmann constant. Here, S is very significant parameter, which gives the strength of electron-phonon coupling. The experimental data is fitted with eqn (2) (Fig. 5(B)) and thus obtained parameters are tabulated in Table 1. The average phonon energy obtained is 17 – 22 meV, which is in close agreement with the bulk value (21.1 meV) of CdTe LO phonons and transverse optical (TO)

(17.23 meV) phonons.[16,33] Interestingly, S increases (Table 1) from 1.13 to 1.53 as the size of QDs decreases 4.8 − 3.0 nm, indicating the stronger coupling between electrons and LO-phonons, which is attributed to the stronger quantum confinement. This increasing value of S with decreasing QDs size is consistent with theoretical prediction and experimental observations.[34] Similar trends i.e., increasing S with decreasing size of QDs was observed in InP/ZnS core-shell structures[35] and a value of 1.5 was reported in Type-I$^{1/2}$ CdTe/CdSe heteronanocrystals.[36] Taking advantage of low temperature PL, we have analyzed effect of temperature on the bandgap of different size QDs. To analyze the size dependence of bandgap, the power law[34] eqn (3) has been used to fit the data as shown in Fig. 6

$$E_g(d) = E_g(\infty) + \frac{A}{d^n}.$$ (3)

Where, $E_g(d)$ is the bandgap of the CdTe QDs of size d at 15 K, $E_g(\infty)$ is the bandgap of bulk CdTe at 4.2 K (1.606 eV)[37] and A is a constant. Fig. 6 shows the shift of bandgap, $E_g(d) - E_g(\infty)$, fitted with eqn (3). The best fitting parameters yields n = 2.1 ± 0.1and A = 5.0 ± 0.8 eV.nm^2. This shows that at low temperatures (15 K), the excitonic bandgap of CdTe QDs has 1/d^2 behavior, which is predicted by effective mass theories considering the direct bandgap nature of the semiconductors.[34]

The temperature induced broadening of PL spectra is another major issue in understanding the optical properties of SNCs. The line-width parameter FWHM is also analyzed to obtain information on the exciton-phonon coupling in the temperaturerange15 − 300 K. FWHM as a function of temperature is shown in Fig. 7 (for particles of different size). It is clearly seen from Fig. 7 that the change in FWHM is quite linear till 70 K, beyond which it increases at relatively faster rate. The broadening of PL can be divided into two different regions,

inhomogeneous and homogeneous which is due to the scattering between exciton-phonon and exciton-impurity/defect as given in the expression below.[38-40]

$$\Gamma(T) = \Gamma_{inh} + \sigma T + \Gamma_{LO}\left(e^{E_{LO}/k_B T} - 1\right)^{-1} + \alpha e^{-E_s/k_B T} \qquad (4)$$

Here, Γ_{inh} is the inhomogeneous broadening parameter due to fluctuations in size, shape, and elemental composition etc. of nanocrystals, which is temperature independent. The two terms that follows represent the homogeneous broadening, which is due to the scattering of excitons with acoustic and optical phonons, respectively. However the last term represents the scattering of excitons by ionized impurity/defect.[39,40] The other parameters in the equation, σ, Γ_{LO}, E_{LO}, α, E_s and k_B are exciton-acoustic-phonon coupling coefficient, the coupling strength of the exciton-LO-phonon, energy of the LO-phonon, linewidth due to ionized impurity/defect scattering, ionization energy of the defect/ionized impurity and Boltzmann constant, respectively. Curve fit by eqn (4) with fitting parameters (Table 2.) is in excellent agreement with the experimental data for nanocrystals of all sizes (Fig. 7).

Interestingly, the value of σ is found to have increasing trend with a maximum 51.1 μeV/K for smaller CdTe QDs (3.0 nm), which is much larger than the theoretical value estimated for bulk (0.72μeV/K).[41] Whereas for CdTe/(Cd,Zn,Te) heterostructures a value of 3.5 μeV/K is reported in a single quantum well (QW) of thickness 18 Å.[42] However this increased exciton-acoustic-phonon coupling coefficient is qualitatively in agreement with the theoretical prediction, which is expected to have an increase in exciton-acoustic phonon coupling in quasi zero-dimensional systems because of quantum confinement.[31] The rise in homogeneous broadening above ~ 70 K is attributed (partially) to the exciton-LO-phonon scattering. As it can be seen from Table 2, Γ_{LO} values obtained for these QDs are smaller (8.9 − 20.3 meV) than the reported bulk values (30

meV[43] and 24 meV[41]). The smaller value of Γ_{LO} in nanostructures compared to bulk is also consistent with the quantum confinement as theoretically predicted and experimentally observed.[31,44] Further, the additional broadening is attributed to the exciton scattering with defect/surface sates.[40] The parameter E_s, which is considered to be activation/ionization energies of impurity or defect states are found to vary between (41 – 75 meV) in theses QDs. Such an effect of broadening because of exciton scattering with ionized impurities has also been observed in quantum systems such as CdSe nanorods[45] and in fluorescent nanoclusters of Au_{10} as well.[46]

To understand the effect of temperature on non-radiative process, which affects the relaxation of excited carriers, we have studied the evolution of PL intensity as a function of temperature in the range of 15 – 300 K. Fig. 8(A) shows an integrated PL intensity as a function of $1/k_B T$. In the case of large size QDs (3.9 – 4.8 nm), PL intensity remains constant till ~ 50 K. However, in the temperature region 50 – 150 K, the PL quenching is relatively slow, beyond which it decreases at a faster rate up to 300 K. Various possible mechanism in the relaxation process of these excited carriers in QDs are radiative, Auger nonradiative scattering,[31,40] Förster resonance energy transfer (FRET) between smaller to lager size QDs, thermal escape of carriers from the dot[47,48] and getting trapped into the surface/defect states.[11,39] However, in these experiments, we have used a CW mode Ar^+ laser source (514.5 nm) of power less than 1 mW focused to ~ 200 μm spot diameter(away from the focal point). Considering the photon fluence (j_p) and the duration of the excited carrier lifetime (Fig. S4), the average number of electron-hole pairs per QD ($< N_0 >$) is found to be much lesser than 1 which is given by $< N_0 > = j_p \, \sigma_0$, where σ_0 is the absorption cross section of the dot.[40] Therefore, the nonradiative carrier relaxation by Auger scattering process can be neglected here.[31] Moreover, we do not find significant difference in the position of PL emission, i.e., QDs in liquid to that of films in solid

state, indicating absence of observable FRET in our samples. Considering the temperature dependent carrier relaxation process, we have used the following model to analyze the PL emission from these QDs where the integrated PL intensity as a function of temperature, $I_{PL}(T)$ is given by[31,49]

$$I_{PL}(T) = \frac{N_0}{1+A(e^{-E_a/k_BT})+B(e^{E_{LO}/k_BT}-1)^{-m}} \quad (5)$$

Where N_0 is the initial carrier population of emitting states (which is also the integrated PL intensity at 0 K), E_a is the activation energy, E_{LO} is the energy of LO phonon, m is the number of LO phonons involved in the thermal escape of carriers and A, B are the pre-exponential factors. The fitted curves with the eqn (5) for different QDs of size 3.9 – 4.8 nm are shown in Fig. 8(A). The best fitted parameters are given in Table 3(I).

Recently, it has been shown that the thermally activated transfer of carriers take place between energy levels of dark and bright excitonic states in CdTe QDs.[50,51] The energy separation for these transitions are less than 10 meV for 3 nm sized QDs and decreases with increase in size.[51] However, such thermally activated transfer of carriers is associated in blue shift of PL peak position[50] (since increase in energy separation) and slight increase in PL intensity[51] with increase temperature up to ~ 50 K. In the larger size QDs (3.9 – 4.8 nm), despite taking PL at a small interval of 5 K in the range 15 – 50 K, we have not observed any blue shift either in PL peak position (Fig. 5) or increase in the intensity (Fig. 8(A)). Therefore the emission properties of such aqueous grown SCNs strongly depend on surface characteristics because of large surface/volume ratio and correspondingly defect density as the size of QDs decreases. Thermal activation energies obtained in our samples are ~ (45 – 19) meV (Table 3(I)) which are quite large than dark-bright exciton separation as discussed earlier. This confirms that the initial

slow decrease in PL intensity with increase in temperature up to 150 K is due to the trapping of carriers in the surface/interface defect states of CdTe/CdS core/shell structure. The deeper understanding of the chemical origin of these trap states and their effect on carrier dynamics is an ongoing intense research and debate topic.[52,53] The presence of Te atoms on the surface of CdTe QDs is widely considered to be a hole trapping center.[54,55] Recently, Califano et al. have shown theoretically the presence of hole trapping centers situated at 50 meV above the valence band position of CdTe QDs due to dangling bonds.[55] The existence of surface states within several tens of meV close to the band edge emission has been reported in non-aqueous grown colloidal CdTe QDs.[56] In thioglycolic acid capped CdTe QDs, the thermal activation energies of 10 and 113 meV have been attributed to the subgap surface states responsible for PL upconversion.[57] Thus, the observed thermal activation energies ~ 45 − 19 meV in this report of MPA capped CdTe QDs indicates the presence of surface traps affecting the PL emission. David J. Binks and co-workers have used chloride ions for effective passivation of surface traps on CdTe QDs and found the domination of radiative recombination's over the nonradiative.[58]

Above 150 K, PL quenching is relatively fast, which limits the quantum efficiency of CdTe QDs at high temperature. Thus the observed PL quenching is attributed to the thermal escape of carriers from the dot assisted by scattering due to multiple LO phonons.[31] It can be seen from the total energy considerations that the contribution from 'm' number of LO phonons $(m \times E_{LO})$ changes from ~ 68 to 90 meV as the QDs size decreases from 4.8 − 3.9 nm (Table 3(I)). In the present investigations of CdTe QDs, the transition corresponding to $1S_{3/2} − 1S_e$ and $2S_{3/2} − 1S_e$ gives the smallest energy difference between two hole-states ($1S_{3/2}$ and $2S_{3/2}$).[59] It is expected that with decrease in QDs size, the energy difference between adjacent states should increase because of stronger confinement.[60] The reported values for energy separation between

adjacent hole-states (1S$_{3/2}$ and 2S$_{3/2}$) are found to be increasing ~ (47 − 120) meV with decrease in QDs size from 4.3 − 2.8 nm.[59] Since the total energy considering multiple LO phonons ~ (68 − 90) meV is comparable to the energy difference between adjacent hole-states of QDs, we attribute the thermal escape of carriers from dot due to the scattering with multiple LO phonons.

Interestingly, for smaller size QDs (3.4 − 3.0 nm) in the temperature range of 15 K to 90 − 130 K there is anomalous behavior in the PL intensity, which increases with increase in temperature. This anomalous behavior, which is not perceived in the relatively larger size QDs (3.9 − 4.8 nm) has been further confirmed by making PL measurements on newly prepared samples of 3.0 nm size QDs (Fig. S5). This anomalous behavior in the PL intensity can be the manifestation of thermally assisted transition from dark to bright exciton states, which are separated by less than 10 meV in energy for 3 nm.[51] However, the possibility of such transition is excluded, since we do not observe any blue-shift in the PL emission in both size QDs (Fig. 5). Therefore, we attribute this thermally activated process to the emission of localized/trapped charge carriers from the CdTe/CdS interface states where the integrated PL intensity can be modified as,[49]

$$I_{PL}(T) = \frac{N_0 + N_0' e^{-\Delta E/k_B T}}{1+(e^{E_{LO}/k_B T}-1)^{-m}},\qquad(6)$$

where, ΔE is the activation energy of these localized/ interface trap states, N_0' is a parameter related to the density of trap states. A well fitted data by the modified eqn (6) using LO-phonon energy equal to 21.1 meV is shown in Fig. 8(B), thus obtained parameters are depicted in Table 3 (II). The potential energy of the localized/ interface states appears to be quite shallow and found to have values around 6 − 13 meV. At this stage, we could not assign such kind of shallow energy parameters to any known defect states in our CdTe based QDs. Such thermally activated

14

carrier de-trapping process and enhancement of average PL lifetime with increasing temperature

was also observed in CdSe/CdS/ZnS multiple core/shell structures.[61] Similar enhancement in PL

intensity with increasing temperature was reported in thiol capped PbS QDs, where carriers

trapped in defect or around the dot overcome the shallow energy barrier and fall into the emitting

ground state of the dot.[62] As the temperature increases beyond 150 K, PL intensity starts to

decrease because of thermal escape of carriers from the dot. As expected the number of phonons

involved in scattering process increases (Table 3(II)) as the particle size decreases to 3.0 nm

(increase in adjacent energy states).[47]

4. Conclusions

In summary, we have investigated the temperature dependent (15 − 300 K) optical

properties of aqueous grown different size CdTe QDs (3.0 − 4.8 nm), which are naturally capped

by CdS shell because of surface stabilizing agent (MPA). XRD and elemental composition

analysis reveals the sulphur enriched region indicating formation CdS on CdTe QDs. Energy gap

follow Varshini relation with the temperature coefficient of $(3.2 − 4.5) \times 10^{-4}$ eV/K.

Huang−Rhys parameter 'S', which gives the strength of the electron-phonon coupling is found to

increase from 1.13 to 1.51 with QDs size varying from 4.8 to 3.0 nm. Partial homogeneous

broadening of line-width is found to be enhanced due to increased exciton-acoustic phonon

coupling coefficient up to 51 μeV/K compared to the bulk value of 0.72 μeV/K in the case of 3.0

nm QDs. To understand the nonradiative processes, which affects the relaxation of carriers, the

integrated PL intensity is observed with increase in temperature. The integrated PL intensity

remains constant till 50 K for relatively large QDs (3.9 − 4.8 nm) beyond which thermally

activated process takes over. Below 150 K a small activation energy, 45 − 19 meV is found to be

15

responsible for quenching of PL suggesting that the emission properties in such aqueous grown SCNs strongly depends on surface characteristics. Above 150 K, the thermal escape of carriers from the dot assisted by scattering with multiple LO phonons is found to be the main mechanism for the fast PL quenching. Interestingly, for smaller size QDs (3.4 – 3.0 nm), the PL intensity is found to enhance as the temperature increases up to 90 – 130 K, which is attributed to the emission of carriers from interface/trap states having activation energy in the range of 6 – 13 meV. Thus the light emitting aqueous grown QDs and the relaxation processes reported here can be of importance for the future technology of optoelectronic devices and biomedical sensors.

Acknowledgment

References

1 L. Brus, *J. Phys. Chem.,* 1986, *90,* 2555.

2 S. M. Reimann and M. Manninen, *Rev. Mod. Phys.*, 2002,**74**,1283.

3 A. P. Alivisatos, *J. Phys. Chem.,*1996, **100***,* 13226.

4 V. L. Colvin, M. C. Schlamp and A. V. Alivisatos, *Nature*, 1994, **370**, 354.

5 N. Tessler, V. Medvedev, M. Kazes, S. Kan and U. Banin, *Science*, 2002, **295**, 1506.

6 R. D. Schaller and V. I. Klimov, *Phys. Rev. Lett.,*2004, **92**, 86601.

7 X. Michalet, F. F. Pinaud, L. A. Bentolila, J. M. Tsay, S. Doose, J. J. Li, G. Sundaresan, A.

M. Wu, S. S. Gambhir and S. Weiss, *Science,* 2005, **307**, 538.

8 V. I. Klimov, A. A. Mikhailovsky, S. Xu, A. Malko, J. A. Hollingsworth, C. A. Leatherdale,

H.J. Eisler and M. G. Bawendi, *Science*, 2000, **290**, 314.

9 G. W. Walker, V. C. Sundar, C. M. Rudzinski, A. W. Wun, M. G. Bawendi and D. G. Nocera,

Appl. Phys. Lett., 2003, **83**, 3555.

10 C. de Mello Donegá, M. Bode and A. Meijerink, *Phys. Rev. B*, 2006, **74**, 085320.

11 Y. Zhao, C. Riemersma, F. Pietra, R. Koole, C. de Mello Donega and A. Meijerink, *ACS*

Nano, 2012, **6**, 9058.

12 X. Xu, Y. Zhao, E. J. Sie, Y. Lu, B. Liu, S. A. Ekahana, X. Ju, Q. Jiang, J. Wang, H. Sun, T.

C. Sum, C. H. A. Huan, Y. P. Feng and Q. Xiong, *ACS Nano*, 2011, **5**, 3660.

13 H. Zhao, H. Liang, F. Vidal, F. Rosei, A. Vomiero and D. Ma, *J. Phys. Chem. C*, 2014, **118**,

20585.

14 T. Schwarzl, E. Kaufmann, G. Springholz, K. Koike, T. Hotei, M. Yano and W. Heiss,

Phys. Rev. B, 2008, **78**, 165320.

15 S. Rawalekar, S. Kaniyankandy, S. Verma and H. N. Ghosh, *J. Phys. Chem. C,* 2010, **114**,

1460.

16 G. Morello, M. De Giorgi, S. Kudera, L. Manna, R. Cingolani, and M. Anni, *J. Phys.*

Chem. C, 2007, **111***,* 5846.

17 Y. Li, L. Jing, R. Qiao and M. Gao, *Chem. Commun. ,*2011, **47**, 9293.

18 V. Lesnyak, N. Gaponik and A. Eychmüller, *Chem. Soc. Rev.,* 2013, **42**, 2905.

19 Q. Zeng, X. Kong, Y. Sun, Y. Zhang, L. Tu, J. Zhao and H. Zhang, *J. Phys. Chem. C,* 2008, **112***,* 8587.

20 W. C. Law, K. T. Yong, I. Roy, H. Ding, R. Hu, W. Zhao and P. N. Prasad, *small* 2009, **5**, 1302.

21 X. Cai, H. Mirafzal, K. Nguyen, V. Leppert and D. F. Kelley, *J. Phys. Chem. C*, 2012, **116**, 8118.

22 A. Samanta, Z. Deng and Y. Liu, *Langmuir* , 2012, **28**, 8205.

23 D. V. Talapin, I. Mekis, S. Götzinger, A. Kornowski, O. Benson and H. Weller, *J. Phys. Chem. B,* **2004,** *108,* 18826.

24 J. Khatei and K.S.R. Koteswara Rao, *Materials Chemistry and Physics*, 2011, **130**, 159.

25 A. L. Rogach, *Materials Science and Engineering B,* 2000, **69–70**, 435.

26 A. L. Rogach, T. Franzl, T. A. Klar, J. Feldmann, N. Gaponik, V. Lesnyak, A. Shavel, A. Eychmüller, Y. P. Rakovich, and J. F. Donegan, *J. Phys. Chem. C,* 2007, **111***,* 14628.

27 N. Gaponik, D. V. Talapin, A. L. Rogach, K. Hoppe, E. V. Shevchenko, A. Kornowski, A.

Eychmüller, and H. Weller, *J. Phys. Chem. B,* 2002, **106**, 7177.

28 Y. P. Varshini, *Physica,* 1967,**34**, 149.

29 L. Brusaferri, S. Sanguinetti, E. Grilli, M. Guzzi, A. Bignazzi, F. Bogani, L. Carraresi, M.

Colocci, A. Bosacchi, P. Frigeri and S. Franchi, *Appl. Phys. Lett.,*1996, **69**, 3354.

30 P. T. K. Chin, C. de Mello Donega, S. S. van Bavel, S. C. J. Meskers, N. A. J. M. Sommerdijk

and R. A. J. Janssen, *J. Am. Chem. Soc.*, 2007, **129**, 14880.

31 D. Valerini, A. Cretí, M. Lomascolo, L. Manna, R. Cingolani and M. Anni, *Phys. Rev. B*,

2005, **71**, 235409.

32 K. P. O'Donnell and X. Chen, *Appl. Phys. Lett.,* 1991, **58**, 2924.

33 D. N. Talwar and M. Vandevyver, *J. Appl. Phys*. 1984, **56**, 1601.

34 A. Narayanaswamy, L. F. Feiner, A. Meijerink and P. J. van der Zaag, *ACS Nano*, 2009, **3**,

2539.

35 A. Narayanaswamy, L. F. Feiner and P. J. van der Zaag, *J. Phys. Chem. C,* 2008, **112**, 6775.

36 E. Groeneveld and C. de Mello Donegá, *J. Phys. Chem. C*, 2012, **116**, 16240.

37 S. Adachi, *Handbook on Physical Properties of Semiconductors, II-VI Compound*

Semiconductors, Vol.3, Chap.14, Kluwer Academic Publishers.

38 J. Lee, E. S. Koteles and M. O. Vassell, *Phys. Rev. B*, 1986, **33**, 5512.

39 P. Yu, X. Wen, Y. R. Toh and J. Tang, *J. Phys. Chem. C,* 2012, **116**, 25552.

40 X. Wen, A. Sitt, P. Yu, Y. R. Toha and J. Tang, *Phys. Chem. Chem. Phys.,* 2012, **14**, 3505.

41 S. Rudin, T. L. Reinecke and B. Segall, *Phys. Rev. B*, 1990,**42**, 11218.

42 E.J. Mayer, N.T. Pelekanos, J. Kuhl, N. Magnea and H. Mariette, *Phys. Rev. B*, 1995, **51**,

   17263.

43 N. T. Pelekanos, H. Haas, N. Magnea, H. Mariette, and A. Wasiela, *Appl. Phys. Lett*., 1992,

   61, 3154.

44 S. Nomura and T. Kobayashi, *Phys. Rev. B*, 1992, **45**, 1305.

45 A. A. Salman, A. Tortschanoff, M. B. Mohamed, D. Tonti, F. V. Mourik and M. Chergui,

   Appl. Phys. Lett., 2007, **90**, 093104.

46 P. Yu, X. Wen, Y. R. Toh and J. Tang, *J. Phys. Chem. C*, 2012, **116**, 6567.

47 M. D. Giorgi, C. Lingk, G. von Plessen, J. Feldmann, S. D. Rinaldis, A. Passaseo, M. D.

   Vittorio, R. Cingolani and M. Lomascolo, *Appl. Phys. Lett*., 2001, **79**, 3968.

48 W. Yang, R. R. L. Webb, H. Lee and P. C. Sercel, *Phys. Rev. B*, 1997, **56**, 13314.

49 P. Jing, J. Zheng, M. Ikezawa, X. Liu, S. Lv, X. Kong, J. Zhao and Y. Masumoto,

   J. Phys. Chem. C, 2009, **113***,* 13545.

50 Y. Nonoguchi, T. Nakashima and T. Kawai, *J. Phys. Chem. C,* 2007, **111***,* 11811.

51 Y. Nonoguchi, T. Nakashima and T. Kawai, *J. Phys. Chem. C* 2008, **112***, 19263.

52 F. M. G. Campos and M. Califano, *Nano Lett.* 2012, **12**, 4508.

53 A. M. Kapitonov, A. P. Stupak, S. V. Gaponenko, E. P. Petrov, A. L. Rogach and A.

Eychmüller, *J. Phys. Chem. B*, 1999, **103**, 10109.

54 S. K. Poznyak, N. P. Osipovich, A. Shavel, D. V. Talapin, M. Gao, A. Eychmüller and N.

Gaponik, *J. Phys. Chem. B*, 2005, **109**, 1094.

55 M. Califano, *ACS Nano*, 2015, **9**,2960.

56 X. Wang, W. W. Yu, J. Zhang, J. Aldana, X. Peng and M. Xiao, *Phys. Rev. B*, 2003, **68**,

125318.

57 Yu. P. Rakovich, S. A. Filonovich, M. J. M. Gomes, J. F. Donegan, D. V. Talapin, A. L.

Rogach and A. Eychmüller, *Phys. Status Solidi B*, 2002, **229**, 449.

58 D. E. Velazquez, M. A. Leontiadou, R. C. Page, M. Califano, P. O'Brien and D. J. Binks,

ChemPhysChem, 2015, **16**, 1239.

59 T. Richard, P. Lefebvre, H. Mathieu and J. Allègre, *Phys. Rev. B*, 1996, **53**, 7287.

60 Y. Masumoto and K. Sonobe, *Phys. Rev. B*, 1997, **56**, 9734.

61 M. Jones, S. S. Lo and G. D. Scholes, *PNAS*, 2009, **106**, 3011.

62 L. Turyanska, A. Patanè, M. Henini, B. Hennequin and N. R. Thomas, *Appl. Phys. Lett.*,

2007, **90**, 101913.
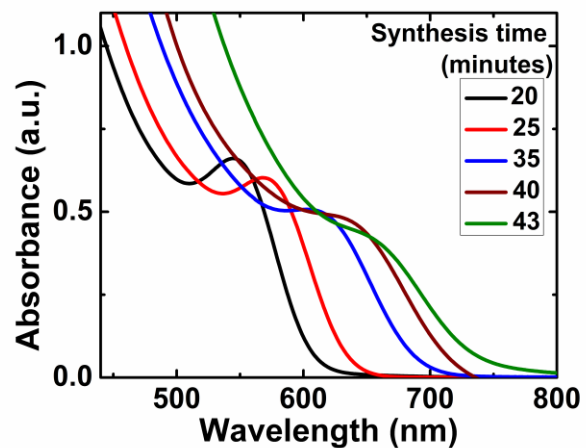
Fig. 1 UV-VIS-NIR absorption spectra of CdTe QDs synthesized for different duration of time by hydrothermal method
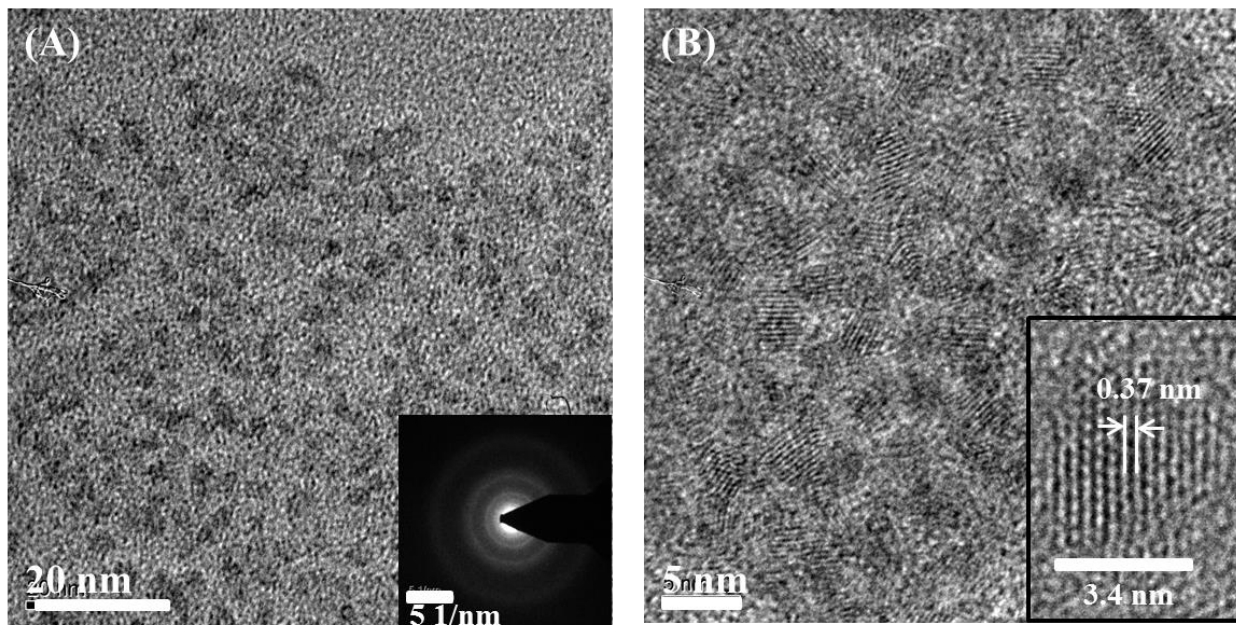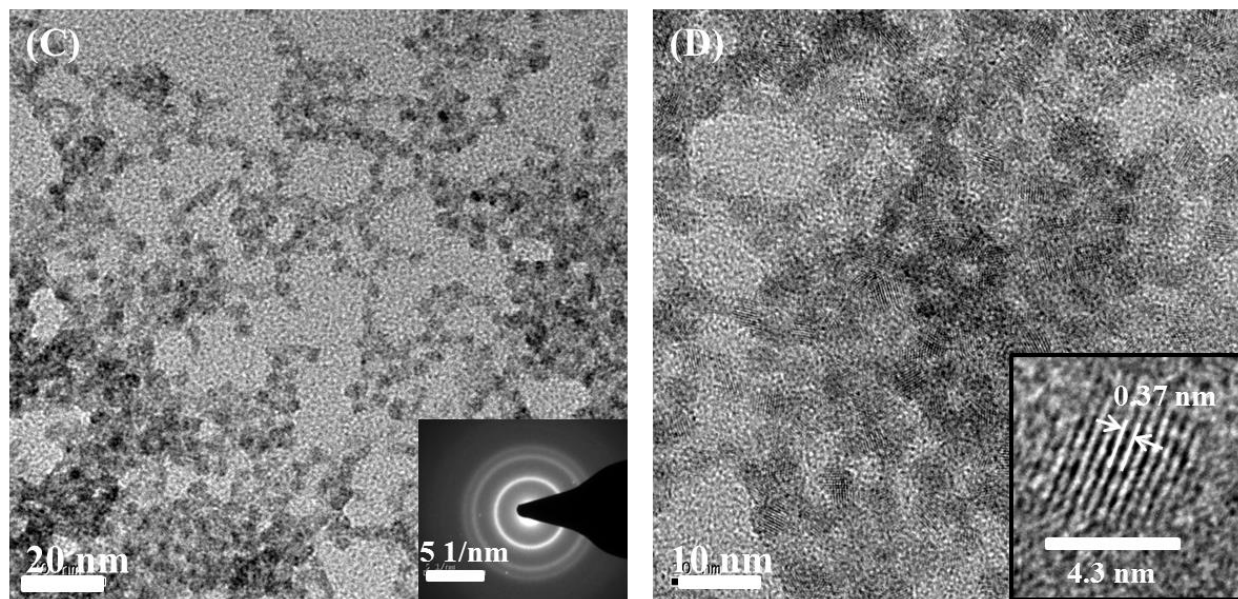
Fig. 2 TEM and HRTEM Images of 25 minutes (A), (B) and 40 minutes (C), (D) synthesized

CdTe QDs, respectively. Inset of (A) and (C) shows electron diffraction pattern for 25 and 40

minutes synthesized QDs, respectively.
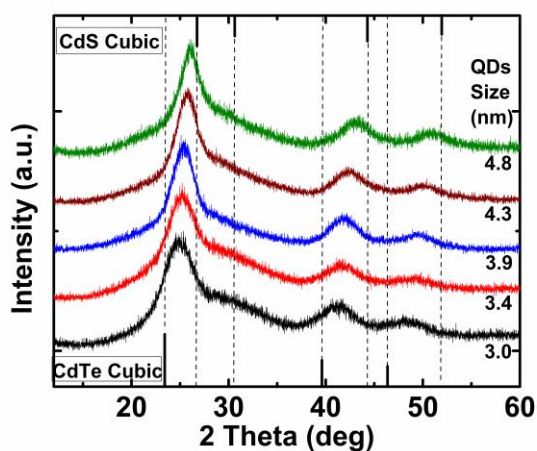
Fig. 3 X-ray diffraction patterns of MPA capped CdTe QDs of size 3.0 – 4.8 nm. The dotted

line is the guideline to the eye.
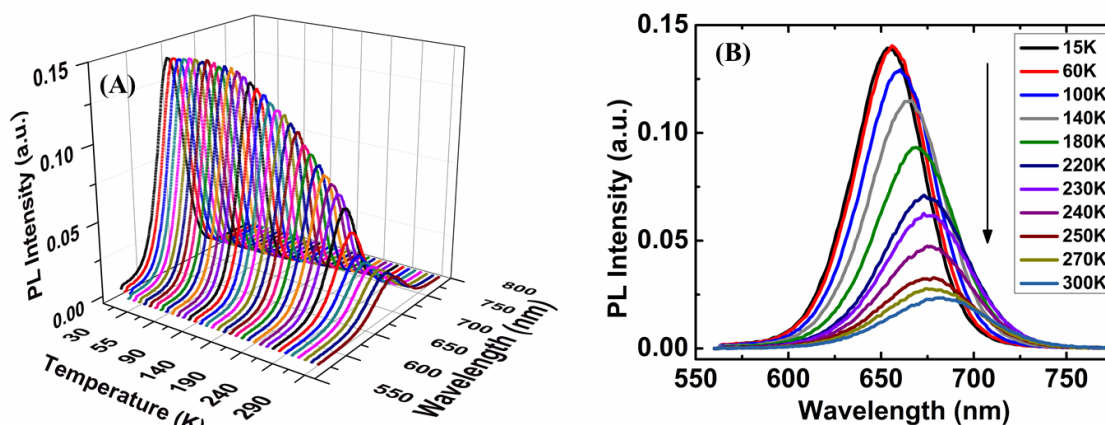
Fig. 4 Evolution of PL spectra with temperature $15 - 300$ K for 3.9 nm QDs (A) 3-D graph showing PL collected at a temperature interval $5 - 10$ K, (B) selected PL showing variation in peak position.
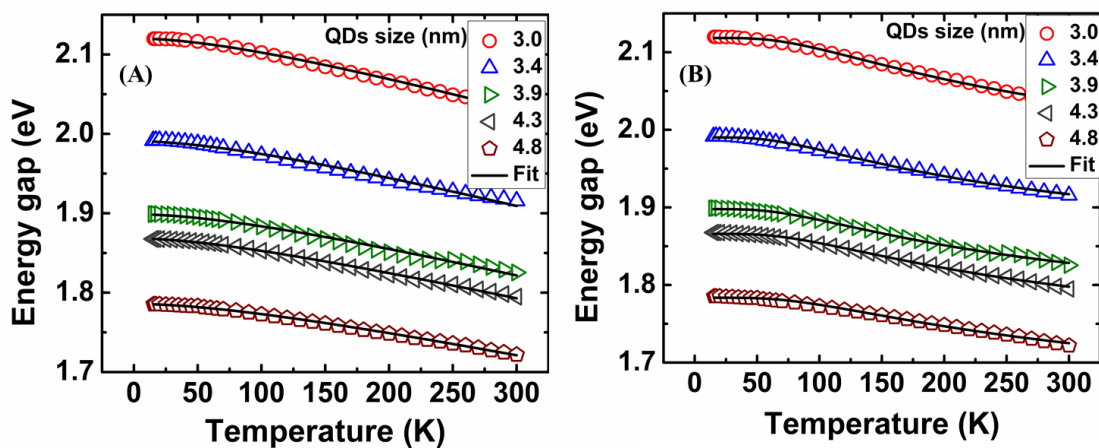
Fig. 5 Energy gap as function of temperature for different size QDs fitted (Solid lines) by (A) Varshini relation eqn (1), (B) O'Donnell and Chen relation eqn (2).
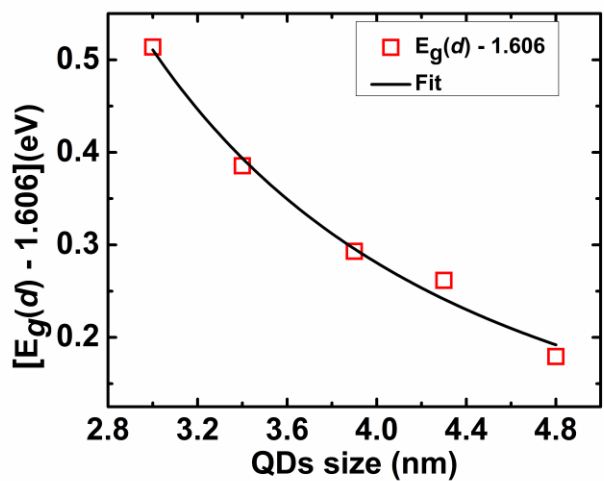
Fig. 6 Bandgap at 15 K as a function of QDs size. The solid line is the curve fitted by eqn (3).
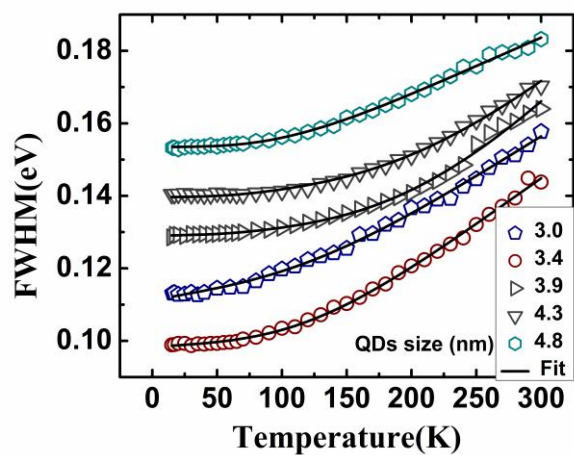
Fig. 7 Temperature dependent FWHM of PL spectra of QDs. Solid line represents the fitted curve by eqn (4).
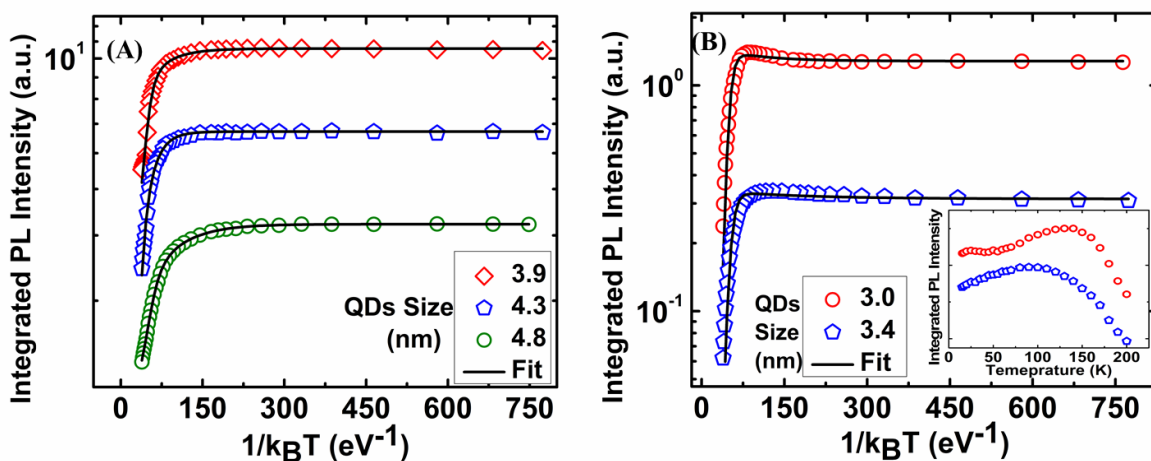
Fig. 8 Integrated PL intensity as a function of $1/k_BT$ for QDs of sizes (A) 3.9, 4.3, 4.8 nm and (B) 3.0, 3.4 nm. Solid line in Fig. (A) and (B) represents the fitted curve by eqn (5) and eqn (6), respectively. Inset of Fig. B shows the integrated PL intensity vs temperature for 3.0 and 3.4 nm QDs.

Table 1 Parameters obtained by fitting O'Donnell and Chen relation eqn (2), energy gap vs temperature.

QDs diameter/nm	E_{g0}/eV	S (Huang-Rhys factor)	$<\hbar\omega>$/meV (Average phonon energy)
3.0	2.09 ± 0.35	1.51 ± 0.01	17.2 ± 0.3
3.4	1.99 ± 0.00	1.46 ± 0.01	19.8 ± 0.4
3.9	1.89 ± 0.39	1.37 ± 0.01	20.7 ± 0.5
4.3	1.86 ± 0.36	1.32 ± 0.01	22.5 ± 0.5
4.8	1.78 ± 0.41	1.13 ± 0.01	24.2 ± 0.7

Table 2 Parameters obtained from eqn (4) fitted to FWHM (Fig. 7) keeping phonon energy E_{LO} (21.1 meV).

QDs diameter /nm	$\sigma/(\mu eV/K)$	$\Gamma_{LO}/$ meV
3.0	51.1 ± 8.5	20.3 ± 2.9
3.4	21.9 ± 6.9	18.7 ± 2.4
3.9	17.1 ± 9.5	8.9 ± 3.3
4.3	4.7 ± 1.6	9.0 ± 0.7
4.8	6.2 ± 2.2	15.2 ± 0.9

Table 3 Parameters obtained from fitted data of temperature dependent integrated PL intensity by **(I)** eqn (5) for 3.9, 4.3 and 4.8 nm size QDs (Fig. 8(A))

QDs diameter/nm	E_a/meV	E_{LO}/meV	m
3.9	25.2 ± 1.6	21.1 ± 0.1	4.3 ± 0.3
4.3	45.4 ± 1.1	21.2 ± 0.4	3.6 ± 0.4
4.8	18.6 ± 0.2	21.1 ± 0.1	3.3 ± 0.1

(II) eqn (6) for 3.0 and 3.4 nm size QDs (Fig. 8(B))

QDs diameter/ nm	ΔE/meV	m
3.0	12.9 ± 2.5	5.5 ± 0.1
3.4	6.4 ± 2.8	5.0 ± 0.1